Optimal Projection Control of an Experimental Truss Structure

Lee D. Peterson*
Purdue University, West Lafayette, Indiana 47907

Optimal projection reduced-order control theory is applied experimentally to a controlled structure testbed. The test structure has 25 disturbed modes, and the controller uses four strain sensors to command four noncollocated stress actuators. The best optimal projection design, an 18th-order controller derived from a 58th-order structural model, is experimentally found to reduce the broad-band vibration of five independent pointing error measures by as much as 66% without saturating the actuators and without destabilizing high-frequency modes. A similar reduced-order linear quadratic Gaussian controller is found to always destabilize high-frequency modes. The homotopy algorithm used to solve the optimal projection synthesis equations is described and its convergence is discussed. Analytical and experimental closed-loop performance for a series of optimal projection controllers are compared to equivalent linear quadratic Gaussian controllers to illustrate the effect of structural dynamic modeling errors on the results.

I. Introduction

ACTIVE control of a structure's dynamic response has become a possible design alternative for reducing the vibration of spacecraft structures. By sensing the motion of the structure and responding through actuator forces at strategic locations, an active controller can regulate the mechanical energy within critical measures, such as the alignment of an optical instrument or the dynamic stress of a critical component. However, the practical use of structural control is hindered by five over-riding design complications: 1) the feedback network must be multi-input/multi-output; 2) many performance measures that cannot be directly sensed must be simultaneously regulated; 3) actuator power is limited and the control effort must be optimized; 4) any available model of the structure will be imperfect; and 5) the controller dimension and sampling rate are limited, whereas the structure is of arbitrarily large order. The controlled structure designer must therefore perform a multiloop design tradeoff that optimizes control effort within the constraints of the control hardware using imperfect models of the system.[1]

Whether such a design is realized depends on the controller synthesis procedure followed. Modern, model-based control design synthesis techniques, such as linear quadratic Gaussian (LQG)[2,3] or H_∞,[4,5] potentially provide systematic solutions to this design problem; that is, they synthesize multiloop designs that feed back sensor outputs through dynamic compensators, simultaneously control many performance measures, and assure best use of actuator power. However, both LQG and H_∞ design methods lead to controllers of dimensions equal to or greater than that of the system being controlled. This hinders the routine application of these methods to structural vibration control. A structure might have 50 or 100 modes that must be controlled, whereas a typical real-time control computer can control no more than 10 or 15 modes at reasonable sample rates. Thus, although modern control methods facilitate efficient design tradeoffs, they do not directly lead to implementable real-time structural control laws.

Several types of controller synthesis methods have been devised to overcome this difficulty.[1,6,7] Indirect methods impose the constraint of controller order separately from the optimization process. They can be classified into two main types. The first type of indirect approach uses model reduction[3] to synthesize a model of dimension equal to the implementable size of the controller. The reduced-order controller is then synthesized from this reduced model. The second type of indirect approach follows an opposite path by first synthesizing a large-order controller from a large-order model. It then uses a controller reduction technique to reduce the controller to an implementable size. Such indirect control design techniques have been extensively developed for LQG objectives,[8,9] and similar indirect techniques can also be envisioned for the H_∞ design. However, because the controller dimension is imposed outside of the design optimization problem, the optimality and guaranteed stability of the controller may be lost in implementation. Indirect controllers are, consequently, suboptimal.

In contrast, direct synthesis methods will remain optimal by generating so-called "fixed-form" controllers.[10,11] Direct methods fix the form of the controller directly within the optimal design equations. These methods synthesize a reduced-order controller from a larger-order model. No intermediate model is required, and no controller reduction is necessary. Direct, fixed-form controllers, therefore, can assure that design objectives are met (for the large-order model) when indirect controllers cannot.

One class of fixed-form controllers which developed from LQG theory is based on the optimal projection (OP) controller synthesis technique.[10] The OP is a mathematical mechanism that incorporates the dimension of the controller hardware into the optimal control design synthesis equations. Consequently, OP leads to controllers of a *specified* dimension that meet the desired optimality conditions for a plant model of a larger dimension. No indirect LQG controller can theoretically perform better than the corresponding OP controller. Originally developed for reduced-order LQG,[10] OP theory has been extended to synthesizing controllers that simultaneously satisfy LQG and H_∞ objectives in the presence of structured and unstructured plant model uncertainties.[6,12] OP, therefore, provides a powerful extension of control design theory for controlling structural vibration by explicitly accounting for controller dimension in the optimization equations.

In the past, the adoption of the OP method has been hindered by the lack of a reliable solution algorithm of the

Received June 27, 1989; presented as Paper 89-3434 at the AIAA Guidance, Navigation, and Control Conference, Boston, MA, Aug. 14–16, 1989; revision received Nov. 7, 1989.

*Assistant Professor of Aeronautics and Astronautics, School of Aeronautics and Astronautics. Senior Member AIAA.

design equations and by the lack of convincing practical experience with the technique. Recently, the numerical solution of the OP equations has been achieved with a homotopy algorithm,[13] and the synthesis of an OP controller for realistic, large-order controlled structures is now practical.[14] Confidence in the OP technique must now come from its experimental application to the control of realistic, nontrivial structures.

This paper presents one such application of OP to an experimental truss structure. The part of OP theory that is applied is the basic extension of LQG theory with a constraint of controller order, originally set forth in Ref. 10. The objective of this study is to examine the design efficiency of OP and compare the achieved closed-loop performance of OP to an indirect LQG method. By providing this comparison on a realistic, experimental structure, this study also focuses on the issues of the practical application of OP using an imperfect dynamic model. A set of OP compensators is designed and tested on the Sandia gamma truss controlled structure testbed.[15] The quadratic performance weighting matrices are found using the output variance constraint (OVC) algorithm.[16] A homotopy algorithm is described, which was implemented in PRO-MATLAB[17] for solving the OP design equations. The performance and robustness of the OP controller are compared to an equivalent reduced-order LQG controller. The LQG controller is developed from an indirect method that uses model reduction followed by controller synthesis.

The principal contributions of this paper are the demonstration and evaluation of the homotopy OP controller synthesis algorithm on a complicated, finite element structural model and the subsequent verification and demonstration of the OP control law on the actual structure. The main conclusion is that OP is a reliable and practical technique, which therefore forms a strong basis for optimal controlled structure design theory. However, OP is observed to retain much of the model parameter error sensitivity contained in LQG. OP controllers with explicit robustness to model parameter error would be preferred for any subsequent application. Furthermore, although not explicitly intended to systematically examine these effects, the results of this study also provide quantitative examples of the impact of modeling errors on the control design process and the achievable performance, as postulated by Skelton.[18]

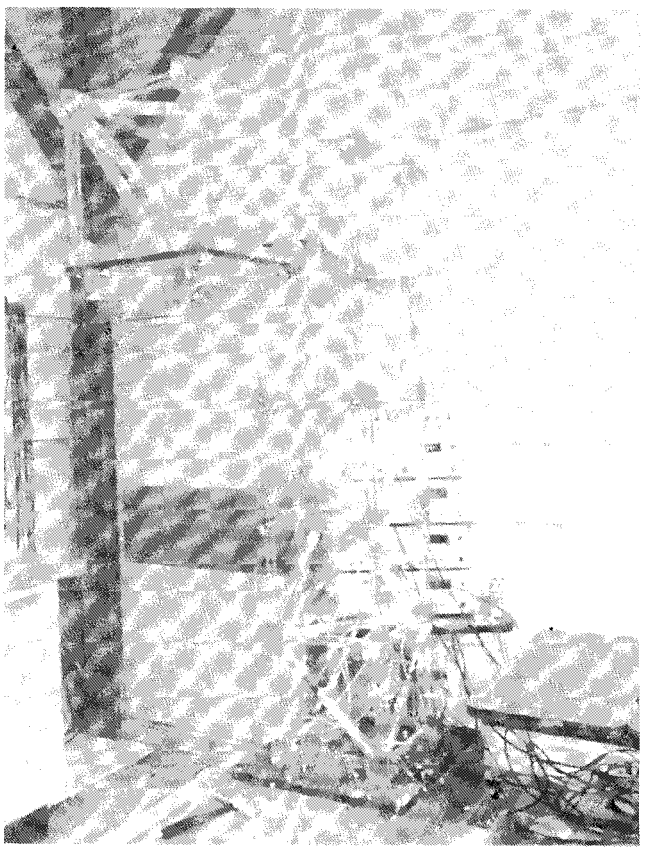

Fig. 1 Sandia gamma truss controlled testbed.

Table 1 Modal frequencies for the Sandia gamma truss structure

Mode	Frequency, Hz
1	10.28
2	10.84
3	19.86
4	21.28
5	45.70
6	60.45
7	62.46
8	78.30
9	88.70
10	115.47
11	131.90
12	138.77
13	144.31
14	150.02
15	162.79
16	171.23
17	175.09
18	177.49
19	182.45
20	194.87

This paper consists of six main sections following this introduction. Sections II and III introduce the experimental apparatus and describe the structural model. The fourth section presents the OP optimal reduced-order control theory. Section V presents in detail the homotopy solution algorithm for solving the OP synthesis equation. The sixth section describes the controller synthesis procedure used in the study, and Sec. VII describes the experimental and analytical results.

II. Sandia Gamma Truss Structure

The Sandia controlled structure testbed (Fig. 1) was developed as part of an internally funded technology development program at Sandia National Laboratories.[15] This research was initiated in 1987 to provide integrated dynamic modeling and control design technology for a wide variety of envisioned programs. By focusing on a specific experiment, this effort provided practical experience in distributed parameter systems control for application on realistic systems. Two major conclusions of this technology development program were 1) the structural control design process is inevitably iterative between experimental test and analytical synthesis, and 2) the associated issues of practical implementation of structural control are critical considerations that have received too little research attention.

The Sandia Gamma Truss Testbed was developed as much as possible without consideration of a particular design technique. Accordingly, the performance objectives, sensors, actuators, and disturbances were purposely not collocated, and the performance measures were not available for feedback. To complicate the design, there are 10 modes within the system bandwidth (amplifier rolloff) of 120 Hz, followed by at least 10 modes within the rolloff band (Table 1). In addition, the structural eigenmodes are closely spaced in pairs.[4] ("Closely-spaced" for control design usually means that small perturbations in the structural model parameters result in large perturbations in the model shapes.) As an example, modes 1 and 2 are the first two modes of the structure. One mode exhibits only slightly more bending than torsion than the other, and the shapes are consequently very similar.

A photograph of the gamma truss is shown in Fig. 1. A five-bay truss segment was cantilevered vertically from a large isolation mass supported by four airbags. A horizontal three-

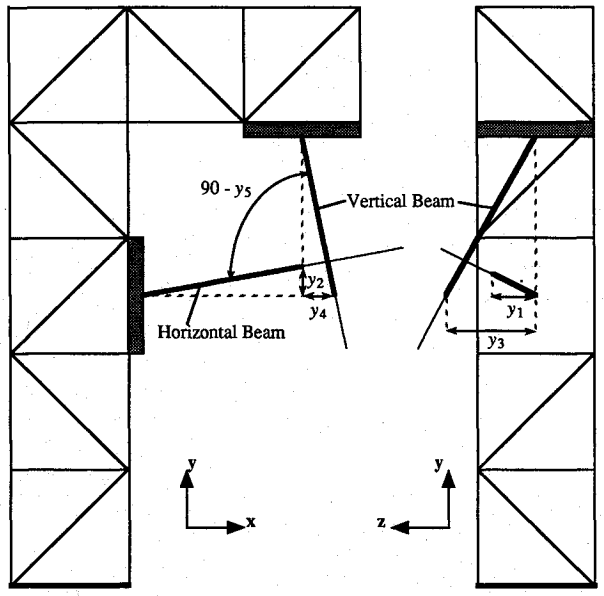

Fig. 2 Diagram of the five performance objectives.

bay segment of the truss was attached to the top of the vertical segment, forming a shape like the Greek letter "Γ." The truss was constructed of polycarbonate tubes 1 in. in diameter and 1/16 in. thick, which were rigidly bonded into universal polycarbonate joining blocks. Each bay of the truss was a 1-ft cube. Bolted to two of the bays were 0.5-in. polycarbonate plates with x-pattern stiffening ribs. The control objective was to minimize the pointing error associated with the intersection of two imaginary beams projecting along the normals to these stiffening plates. This pointing error is defined by five independent performance criteria (Fig. 2): 1) y_1—z alignment error of the horizontal beam, 2) y_2—y alignment error of the horizontal beam, 3) y_3—z alignment error of the vertical beam, 4) y_4—x alignment error of the vertical beam, and 5) y_5—error from perpendicularity of the beam intersection. Although the beams do not theoretically intersect, y_5 is formed assuming that they do by projecting the beams into an appropriate two-dimensional plane. The performance measures were synthesized from a set of signals from accelerometers positioned on the x-pattern stiffening plates. The design disturbance was a force applied at the upper corner of the truss directed into the center of the top truss bay.

The vibration was sensed by four axial strain sensors and was controlled by four axial stress actuators, as indicated in Fig. 2. The feedback sensors were four piezoelectric polymer strain gauges attached to the diagonal struts in the second bay from the base of the truss. The polymer sheets were wrapped around and bonded to the trusses. Through a charge amplifier, each sensor produced a voltage proportional to the axial strain in its truss diagonal. The actuators were piezoelectric ceramic (lead magnesium niobate) bonded to the outside of the four diagonals in the bottom bay of the truss structure.[19,20] Each actuator produced an axial stress in its diagonal truss member proportional to its input voltage. The actuator power supplies had a bandwidth of 120 Hz. The sensor and actuator gains could be balanced so the motion-induced near actuator saturation also saturated the sensors.

The digital controller was a Systolic PC-1000 array processor operating at a peak cycle rate of 2000 samples and updates per second. This produced a phase lag of 18 deg at the 3 dB rolloff of the actuator power supplies. The PC-1000 could accommodate an 18-state control law, and this dimension was always used in the experiments.

III. Synthesis of an Appropriate Structural Model

The formulation of the structural dynamic model onto which the control design is based will ultimately limit the achievable closed-loop performance.[18] Because the size of the structural model for control design is usually limited by computational resources, the content of the model must be carefully selected to include only those dynamic components (degrees of freedom) that most affect the input-output fidelity of the model. The content of the structural model, therefore, uniquely depends on the performance objectives, the sensor-actuator configuration, and the disturbances.[3] Open-loop accuracy, however, is not sufficient to yield good closed-loop performance.[18] Rather than an *accurate* model, the designer must seek an *appropriate* model for the controller design. Since this is a priori impossible without a pre-existent controller, the selection of a design model and the design of the controller are necessarily iterative. The experience of this research supports these assertions.

Initially, it was assumed that an open-loop accurate model is sufficient for control design. A finite element model was developed that predicted the modal parameters within a few percent. However, this initial, presumably accurate design model yielded an unstable closed-loop baseline LQG control. It was only then realized that the high accuracy assumed in the open-loop model was not valid with the controller operating. The first two mode shapes in the analytical model were sufficiently in error to confuse the controller and consequently drive the system unstable. A small phase error, *unimportant to the open-loop L_2 norm of the model error*, was resulting in arbitrarily large closed-loop errors. This confirms experimentally such an assertion made by Skelton in Ref. 18.

Because of this, much effort was invested in this research toward verifying and updating the structural model with experimental testing. System identification was used to revise the finite element model of the structure according to the following procedure. The structural model was based on a 1900 DOF MSC-NASTRAN[21] finite element model. A parameter identification technique updated the elastic modulus and boundary conditions of the finite element model using experimental modal data.[22] With this procedure, the finite element model reproduced the experimental modal frequencies of the open-loop system to high precision. Of the first 10 modal frequencies, 5 were accurate to within $<1\%$, as indicated in Table 2. In addition, the experimentally determined modal damping values for the first 10 modes were used in the model, with an appropriate Rayleigh damping model for the modes above mode 10. This model would be considered by many experimentalists to represent the highest precision, which should be reasonably expected for a finite element structural model. It should be noted that this model was simply the best achievable with the system identification method used, and it was not necessarily the most appropriate model achievable for the control design.

Beginning with the updated finite element model, an evaluation model for controller synthesis was developed in two steps. The 1900 DOF model was first reduced to an eigensolvable dimension (216 DOF) via a NASTRAN ASET static reduction.[21] An eigenanalysis was performed on this model to produce a 432-state structural model in the standard form.

Table 2 Improvement in modal frequencies via system identification

Mode number	Initial errors, %	After update No. 1, %	After update No. 2, %
1	8.04	2.38	0.00
2	5.24	4.91	0.28
3	7.56	2.80	2.72
4	12.50	1.64	0.28
5	12.00	1.23	0.37
6	8.46	1.98	1.87
7	13.5	2.58	0.93
8	12.18	1.10	1.19
9	9.52	1.14	2.04
10	16.19	4.52	3.30

This was translated into PRO-MATLAB[17] matrices through a special-purpose program called NASMAT.[23] The dimension of this model was too large for a controller synthesis evaluation model and contained much unimportant dynamic information. The size of the evaluation model derived from the 432-state model was determined by a combination of system bandwidth, model reliability, modal observability and controllability, and modal cost analysis.[3] The 432-state model was reduced to a 58-state model using these criteria. The resulting truth model or evaluation model included 50 structural states, 4 amplifier rolloff states, and 4 digital processing delay states. This model was the basis for the controller synthesis.

IV. Optimal LQG Reduced-Order Control Theory

The reduced-order LQG design problem considered here is to find the dynamic compensator

$$\dot{x}_c = A_c x_c + F z \tag{1}$$

$$u = K x_c \tag{2}$$

with n_c internal states x_c, which feeds back sensor outputs z into control actuator signals u to force the presumed system model

$$\dot{x} = Ax + B_u u + B_w w \tag{3}$$

$$z = Mx + v \tag{4}$$

$$y = Cx \tag{5}$$

with n states x so that the following quadratic performance cost functional is minimized:

$$J = E_\infty[y^T R_1 y + u^T R_2 u] \tag{6}$$

in the presence of specified white noise disturbances w and sensor noise v, for which

$$E_\infty(w) = 0, \qquad E_\infty(ww^T) = W \tag{7}$$

$$E_\infty(v) = 0, \qquad E_\infty(vv^T) = V \tag{8}$$

The notation $E_\infty(f)$ means the expected value of $f(t)$. The weighting matrices R_1 and R_2 can be determined to satisfy certain covariance constraints:

$$E_\infty(y_i^2) \le \bar{\sigma}_{yi}^2 \tag{9}$$

while minimizing control effort

$$\sum_i E_\infty(u_i^2) \tag{10}$$

by the solution to an auxiliary problem that involves iterative solution of the closed-loop, full order, LQG compensator.[16]

When the order of the compensator is the same as the order of the plant,

$$n_c = n \tag{11}$$

the solution to the preceding LQG problem is the well-known Kalman filter state estimator coupled to the linear quadratic regulator, for which[2,3]

$$A_c = A - Q\bar{\Sigma} - \Sigma P \tag{12}$$

$$F = QM^T V^{-1} \tag{13}$$

$$K = -R_2^{-1} B_u^T P \tag{14}$$

where F is the Kalman filter optimal state estimator gain and K is the optimal regulator state feedback gain, and

$$\bar{\Sigma} = M^T V^{-1} M \tag{15}$$

$$\Sigma = B_u R_2^{-1} B_u^T \tag{16}$$

The matrices Q and P are given by the solution to the following Riccati equations:

$$AQ + QA^T + B_w W B_w^T - Q\bar{\Sigma}Q = 0 \tag{17}$$

$$A^T P + PA + C^T R_1 C - P\Sigma P = 0 \tag{18}$$

Notice that Eqs. (17) and (18) for Q and P and, hence, those of the estimator F and the regulator K are uncoupled. This is due to the so-called separation principal of full-state feedback optimal control.[2] Such a compensator is guaranteed stable (when the solution exists) in the absence of modeling errors. Of course, for a theoretically infinite, order distributed parameter system such as a structure, the assumption $n = n_c$ is potentially the single most dangerous modeling error.

Hyland and Bernstein[7,10] derived the necessary stationary conditions that extend the previous LQG theory to account for a reduced-order compensator:

$$n_c \le n \tag{19}$$

If we perform the cost minimization for the LQG problem statement, but include a constraint on the order of the compensator, the optimal, reduced-order compensator can be shown to be

$$A_c = \Gamma[A - Q\bar{\Sigma} - \Sigma P]G^T \tag{20}$$

$$F = \Gamma Q M^T V^{-1} \tag{21}$$

$$K = -R_2^{-1} B_u^T P G^T \tag{22}$$

These equations are only slightly different in form to the full-order LQG Eqs. (12-14). The new matrices Γ and G are rectangular matrices that depend on a projection matrix presented below. The matrices Q and P are also given by equations similar in form to the Kalman filter and optimal regulator Eqs. (17) and (18):

$$AQ + QA^T + B_w W B_w^T - Q\bar{\Sigma}Q + Q\bar{\Sigma}Q\tau_\perp^T = 0 \tag{23}$$

$$A^T P + PA + C^T R_1 C - P\Sigma P + \tau_\perp^T P \Sigma P \tau_\perp = 0 \tag{24}$$

in which the projection operator matrix is given by

$$\tau = G^T \Gamma \tag{25}$$

$$\tau_\perp = I_n - \tau \tag{26}$$

This projection matrix is a reduced rank idempotent operator:

$$\text{rank}\ \tau = n_c \tag{27}$$

which means[10]

$$\tau^2 = \tau \tag{28}$$

When $n_c = n$, the projection operator τ becomes the identity matrix. Hence, $\tau_\perp$ becomes $\mathbf{0}$, and the OP compensator is identical to the full-order LQG Kalman filter/optimal regulator controller. The projection matrix τ and, hence, its factors G and Γ are determined by a particular eigenfactorization of the product of two more matrices, $\hat{Q}$ and $\hat{P}$, which is written symbolically as[7,14]

$$\tau = \sum_{k=1}^{n_c} \prod_k [\hat{Q}\hat{P}] \tag{29}$$

The matrices $\hat{Q}$ and $\hat{P}$ satisfy the following matrix equations:

$$(A-\Sigma P)\hat{Q}+\hat{Q}(A-\Sigma P)^T+Q\bar{\Sigma}Q-\tau_\perp Q\bar{\Sigma}Q\tau_\perp^T=0 \quad (30)$$

$$(A-Q\bar{\Sigma})^T\hat{P}+\hat{P}(A-Q\bar{\Sigma})+P\Sigma P-\tau_\perp^T P\Sigma P\tau_\perp=0 \quad (31)$$

These equations for $\hat{Q}$ and $\hat{P}$ are similar to the equations for observability and controllability grammians found in full-order LQG theory.[3]

The projection operator τ is the mathematical device that performs the reduction from the full-order model size n to the compensator size n_c. From its relation with the observability and controllability grammians $\hat{Q}$ and $\hat{P}$, τ projects onto the controller the most observed and most controlled subspace of the plant and, thereby, assures optimality of the reduced-order compensator.

The two equations [Eqs. (17) and (18)] for Q and P in full-order LQG theory have been replaced by Eqs. (23), (24), (30), (31), and (29) for Q, P, $\hat{Q}$, $\hat{P}$ and τ. Once these have been solved, the G and Γ factors of τ are given by the conditions of Eqs. (25), (27), and (28) to complete the determination of the compensator gain matrices, A_c, F, and K. Notice also that for this optimal reduced-order controller, the synthesis equations are fully coupled, indicating that the separation principle of full-order LQG design does not apply to a reduced-order design. This means that the states of the compensator are not estimates of the states of the structure, as they are for the Kalman filter/optimal regulator full-order controller. This coupling highlights the fact that modeling and control design are coupled processes.

V. Homotopy Algorithm for Solution of the OP Equations

The solution of the OP equations consists of finding the zeros of the five coupled, nonlinear, matrix equations given previously. Because there is no closed-form solution to these equations, a numerical technique must be used. This section presents the *discrete* homotopy algorithm that was implemented in PRO-MATLAB as a special purpose M-file program to solve the OP synthesis equations. The algorithm is based on the technique presented in Refs. 7, 24, and 25. The algorithm presented here is efficient enough for small problems, but becomes unwieldy for larger ones. It typically required 45 min of VAX 8700 CPU time to synthesize an 18-state controller from a 58-state system model. A newer, more efficient *continuous* homotopy algorithm has been devised that avoids the pathologies of the algorithm used here.[13] As a result, it may prove to be an order of magnitude faster and should always find a solution when it exists. The basic structure of the simpler algorithm presented here is the same as the newer algorithm.

The homotopy approach to finding the zeros of algebraic nonlinear problems is based on rigorous, topological continuation theory, but is conceptually very simple.[25] Suppose there is some nonlinear function $f(x)$ for which we desire to know the zeros; i.e., we wish to solve

$$f(x)=0 \quad (32)$$

for x. Usually, we can separate f into a part f_s, which has a simple solution, and the remainder f_t, which is the cause of all the trouble

$$f(x)=f_s(x)+f_t(x) \quad (33)$$

Now, define an auxiliary function $g(\alpha,x)$ by multiplying the troublesome part of $f(x)$ by some parameter α:

$$g(\alpha,x)=f_s(x)+\alpha f_t(x) \quad (34)$$

Now, note that

$$g(0,x)=f_s(x) \quad (35)$$

which, by design, has an easy or known solution, and also note that

$$g(1,x)=f_s(x)+f_t(x)=f(x) \quad (36)$$

The homotopy algorithm for finding the zeros to $f(x)$ is then as follows. Beginning at the known solutions at $\alpha=0$, follow the paths of solutions as α varies from 0 to 1. When α reaches 1, the solutions are the desired zeros of $f(x)$.

The two general types of homotopy algorithms are distinguished according to how the solution path along α is followed. The "discrete" homotopy methods step α through in discrete values, with an iterative solution at each value of α starting with the most recent solution found. The "continuous" homotopy methods write the differential equation for $g(\alpha,x)=0$ in the direction of α and then solve the algebraic problem by integrating this ordinary differential equation from $\alpha=0$ to 1. For the OP equations, the continuous algorithm is far more efficient to use, but much more difficult to program. The discrete algorithm was used in this research for simplicity in programming.

To solve for the OP controller, we desire to find Q, P, $\hat{Q}$, $\hat{P}$, and τ, the solutions to the OP Eqs. (23), (24), (30), (31), and (29). The homotopy solution of these equations involves a homotopic deformation of two terms in the equations for Q and P, Eqs. (23) and (24), through the use of two independent homotopy parameters, α and β. The homotopic parameterized form of the OP equations is chosen to be as follows:

$$AQ+QA^T+\beta B_w WB_w^T-Q\bar{\Sigma}Q+\alpha\tau_\perp Q\bar{\Sigma}Q\tau_\perp^T=0 \quad (37)$$

$$A^TP+PA+\beta C^TR_1C-P\Sigma P+\alpha\tau_\perp^T P\Sigma P\tau_\perp=0 \quad (38)$$

$$(A-\Sigma P)\hat{Q}+\hat{Q}(A-\Sigma P)^T+Q\bar{\Sigma}Q-\tau_\perp Q\bar{\Sigma}Q\tau_\perp^T=0 \quad (39)$$

$$(A-Q\bar{\Sigma})^T\hat{P}+\hat{P}(A-Q\bar{\Sigma})+P\Sigma P-\tau_\perp^T P\Sigma P\tau_\perp=0 \quad (40)$$

$$\tau=\sum_{k=1}^{n_c}\prod_k[\hat{Q}\hat{P}] \quad (41)$$

The first homotopy parameter α multiplies the reduced rank part of the Q and P equations, without which Eqs. (23) and (24) would be the same as the full-order Riccati equations (17) and (18). Thus, α allows the solutions to start with the full-order controller solution and slowly reduce the rank of τ. When α is 1, the optimal projection reduction to the controller dimension of n_c is complete. The second homotopy parameter β effectively softens the gain requested from the controller. Numerical difficulties are often encountered when there is high disturbance level W (equivalent to low sensor noise V) or high performance weight R_1 (equivalent to low control effort weight R_2). Either of these conditions is ordinarily referred to as a "high-gain" controller. The β parameter, therefore, allows the algorithm to begin at a gain for which the solution is reliably found and then ease into the high gain solution. It should be noted that the numerical difficulties encountered for the high-gain controller are encountered for any LQG controller synthesis method, including the full-order LQG solution. It is true, in general, that the more gain asked for from the controller, the more difficult the solution to the optimum necessary conditions.

The discrete homotopy solution algorithm is as follows (see Fig. 3):

1) Initialize α to 0.
2) Initialize β to a small value (β_0), which allows solution of the full-order Riccati equation.
3) Initialize τ to the identity matrix I_n and, therefore, $\tau_\perp$ to the zero matrix 0_n.
4) β loop
   a) α loop

i) Solve the following equations for Q and P beginning with the last solutions for Q, P, and τ:

$$AQ + QA^T + \beta B_w W B_w^T - Q\bar{\Sigma}Q + \alpha\tau_\perp Q\bar{\Sigma}Q\tau_\perp^T = 0 \quad (42)$$

$$A^T P + PA + \beta C^T R_1 C - P\Sigma P + \alpha\tau_\perp^T P\Sigma P\tau_\perp = 0 \quad (43)$$

When α is zero, this is a simple Riccati solution. Otherwise, this involves an iterative solution procedure in which the $j+1$ iterates are given by the following Lyapunov equation[26]:

$$(A - Q_j\bar{\Sigma})Q_{j+1} + Q_{j+1}(A - Q_j\bar{\Sigma})^T + \beta B_w W B_w^T + Q_j\bar{\Sigma}Q_j + \alpha\tau_\perp Q_j\bar{\Sigma}Q_j\tau_\perp^T = 0 \quad (44)$$

$$(A - \Sigma P_j)^T P_{j+1} + P_{j+1}(A - \Sigma P_j) + \beta C^T R_1 C + P_j\Sigma P_j + \alpha\tau_\perp^T P_j\Sigma P_j\tau_\perp = 0 \quad (45)$$

Convergence is achieved when the 1 norm of the residual in the modified Riccati equation is below some specific tolerance (usually $<1\%$) of the 1 norm of the solution.

ii) Solve the following Lyapunov equations for $\hat{Q}$ and $\hat{P}$ using the converged solutions for Q and P and the last τ:

$$(A - \Sigma P)\hat{Q} + \hat{Q}(A - \Sigma P)^T + Q\bar{\Sigma}Q - \tau_\perp Q\bar{\Sigma}Q\tau_\perp^T = 0 \quad (46)$$

$$(A - Q\bar{\Sigma})^T\hat{P} + \hat{P}(A - Q\bar{\Sigma}) + P\Sigma P - \tau_\perp^T P\Sigma P\tau_\perp = 0 \quad (47)$$

iii) Find the eigenvectors and eigenvalues of $\hat{Q}\hat{P}$. The computations are a source of numerical difficulty since, as the rank of τ approaches n_c, many of the eigenvalues of $\hat{Q}\hat{P}$, which should be zero, are numerically complex numbers and need to be explicitly set to zero.

iv) Sort the right eigenvectors U, the left eigenvectors V, and the vector eigenvalues E in order of decreasing eigenvalues. This ranks the eigenvectors by their observability and controllability.

v) Orthonormalize U and V so that

$$V^T U = I \quad (48)$$

vi) Form the diagonal matrix of eigenvalue ratios γ defined by

$$\gamma_i = \begin{cases} 1, & i \le n_c \\ E_i/E_{n_c}, & i > n_c \end{cases} \quad (49)$$

Note that as the rank of τ approaches n_c, the desired condition, the $n_c + 1$ to n values of γ approach zero. The rank of τ is indicated by the value of γ_{n_c+1}.

vii) Form the projection τ according to

$$\tau = U\gamma V^T \quad (50)$$

b) If $(\alpha\beta)\gamma_{n_c+1} > 0.01$, repeat the solution for Q, P, $\hat{Q}$, and $\hat{P}$ without incrementing α or β.

c) If $\alpha = 0$, then increment α and loop.

d) If 1) $\alpha = 1$, or 2) the computed loop cost J_{n_c} is within an acceptable tolerance (usually $<1\%$) of the full-order closed-loop cost for the current value of β, or 3) the cost is not significantly decreasing with each iteration, end the α loop and increment β.

5) If $\beta = 1$ then end the β loop, otherwise increment β and loop.

6) Form Γ and G, the factors of τ:

$$\Gamma = [I_{n_c} 0]V^T \quad (51)$$

$$G = [I_{n_c} 0]U^T \quad (52)$$

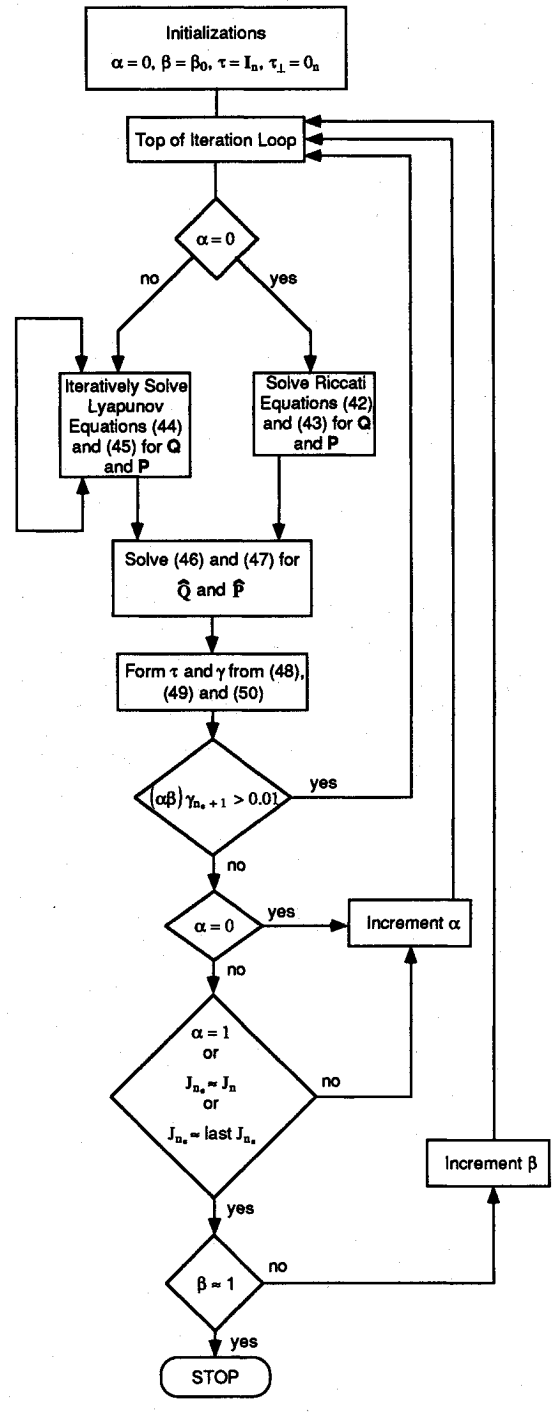

Fig. 3 Flowchart of the OP homotopy solution algorithm.

7) Compute the compensator matrices

$$A_c = \Gamma[A - Q\bar{\Sigma} - \Sigma P]G^T \quad (53)$$

$$F = \Gamma QM^T V^{-1} \quad (54)$$

$$K = -R_2^{-1}B_u^T PG^T \quad (55)$$

The most important part of this algorithm is determining suitably small increments in α and β to insure iterative solvability of the Q and P homotopy equations. A cutback algorithm was used successfully in this research. The homotopy step increment, $\Delta\alpha$ or $\Delta\beta$, was halved whenever a step led to a divergent solution for Q and P. Initial steps of $\Delta\alpha = 1$ or $\Delta\beta = 1$ were used.

It is useful to show how the rank of the optimal projection matrix τ was reduced as the homotopy algorithm converged.

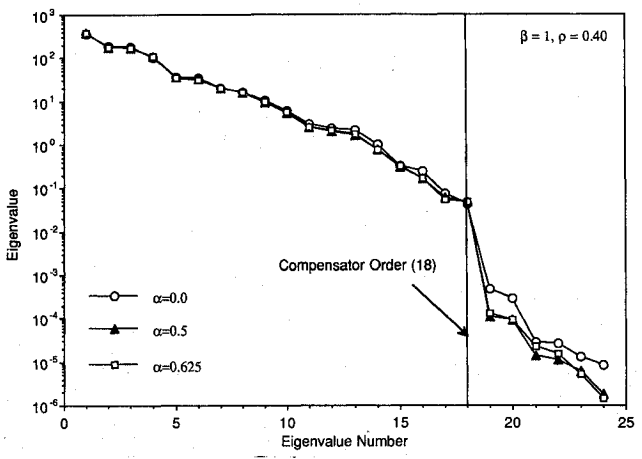

Fig. 4 Observability-controllability eigenvalues vs eigenvalue number, demonstrating the reduced rank jump at the specified controller dimension, $n_c = 18$.

As the solution is approached, the rank of τ approaches n_c. This is illustrated in Fig. 4 by plotting the entries of the eigenvalue vector E for increasing values of α when β is 1. The data is taken from one of the OP compensators designed in this research, according to the procedure described in the next section. Note the drop in two orders of magnitude at $i = 18 = n_c$, the compensator dimension. When the magnitude of this drop is more than a factor of 100, the rank of τ has converged to the required value of n_c. In this case, this happens when $\alpha = 0.625$.

VI. Controller Synthesis Procedure

Within the context of the control theory reviewed, two sets of reduced-order controllers were derived for the Sandia gamma truss. The first were designed following an indirect procedure, in which the full-order LQG theory is applied to an 18-state, reduced-order model. The second used the optimal projection synthesis equations, which used the full-order, 58-state evaluation model. These procedures are specified later. All the synthesis calculations were performed with special purpose PRO-MATLAB M-file programs.[17]

Suboptimal LQG_{n_c} Compensator Synthesis

This technique follows one indirect synthesis approach described in the Introduction: reduce the evaluation model by excluding all but n_c states, and then apply LQG to the reduced-order model. The steps in the procedure are the following:

1) Specify the disturbance covariance matrix W and sensor noise covariance matrix V.

2) Form the reduced system model by selecting the n_c states with the highest modal cost.[3]

3) Compute the open-loop rms response of the full-order system model.

4) Specify the desired closed-loop response as a fraction of the open-loop response

$$E_\infty(y_i^{CL})^2 \le \rho^2 E_\infty(y_i^{OL})^2 \qquad (56)$$

The scalar ρ is the desired improvement in the closed-loop performance.

5) Find the LQG weighting matrices to satisfy the desired closed-loop performance. This is done iteratively using the output covariance constraint (OCC) algorithm.[16]

6) Formulate the reduced-order compensator using the LQG equations. The solution to these equations is a standard function call in PRO-MATLAB.

7) Couple the compensator to the full-order system model. Compute the eigenvalues and closed-loop response of the system using the full-order evaluation model.

Repeat this procedure from step 4 with successively smaller values of ρ until one of the following criteria is satisfied: 1) the reduced-order compensator destabilizes the full-order system model, or 2) the actuators are saturated.

Optimal Projection Compensator Synthesis

The synthesis of the OP controller is carried out in parallel with the suboptimal LQG_{n_c} controller. To facilitate comparison with the LQG_{n_c} controllers, the same weighting matrices are used in the OP synthesis as is the LQG_{n_c} synthesis for a given specified value of ρ. The steps in the synthesis procedure are the following:

1) Use the disturbance covariance matrix and sensor noise covariance matrix specified in the LQG_{n_c} procedure.

2) Use the same weighting matrices determined for each compensator designed in the LQG_{n_c} procedure. This provides parallel comparison between OP and LQG_{n_c} controllers.

3) Solve the OP equations. This is done within a special purpose PRO-MATLAB M-file program, which implements the previous homotopy algorithm.

4) Couple the compensator to the full-order system model. Compute the eigenvalues and closed-loop response of the system using the full-order evaluation model.

Repeat this procedure from step 2 until one of the following criteria is satisfied: 1) the actuators are saturated, or 2) the homotopy algorithm does not converge. In practice, both conditions usually occurred simultaneously.

VII. Comparison of Experimental and Analytical Results

With this procedure, eight controllers (three OP and five LQG_{n_c}) were synthesized and implemented on the Sandia gamma truss. The closed-loop stability for these controllers is summarized in Table 3. Each controller is parameterized by a particular value of ρ and an associated control design method, OP or LQG_{n_c}. At high ρ (low gain), both the LQG_{n_c} and OP sets of controllers were stable. At approximately $\rho = 0.30$, however, the LQG_{n_c} controllers became unstable. At low ρ (high gain), an LQG_{n_c} controller will destabilize modes that were excluded from the reduced-order synthesis model. At first, this results in degraded performance, but eventually it results in an unstable closed-loop system. This destabilization of modes not contained within the control design model is usually called "spillover." In contrast, the OP algorithm always produced controllers that never destabilized high-frequency modes contained in its higher-order design model. However, OP controllers could not be synthesized below $\rho = 0.33$ because the discrete homotopy algorithm failed to converge.[5] (This pathology is reportedly not encountered with the newer continuous homotopy algorithms.[13])

Before comparing the performance of each of the stable controllers, it is important to consider what is a proper measure of controller performance. The algorithm developed earlier sought to constrain the rms broad-band response of each y_i individually while minimizing control effort. This is the criteria used here. Other measures often used as performance measures include the transient decay of a particular

Table 3 Stability of controllers synthesized with the LQG_{n_c} and OP algorithms

	LQG_{n_c}		OP	
ρ	Analytical	Experimental	Analytical	Experimental
0.50	S[a]	S	S	S
0.40	S	S	S	S
0.33	S	S	S	S
0.30	S	S	—	—
0.28	S	U[b]	—	—
0.27	U	—	—	—
0.25	U	—	—	—
0.20	U	—	—	—
0.10	U	—	—	—

[a]S = stable. [b]U = unstable.

Table 4 Closed-loop performance for $\rho = 0.33$

Performance measure	Open-loop	Full-order LQG	LQG_{n_c}		OP	
			Predicted	Observed	Predicted	Observed
y_1	1.00	0.32	0.65	0.60	0.34	0.45
y_2	1.00	0.34	0.45	0.45	0.34	0.34
y_3	1.00	0.35	0.45	0.50	0.36	0.50
y_4	1.00	0.33	0.35	0.55	0.33	0.44
y_5	1.00	0.38	0.59	0.83	0.40	0.64

mode or the narrow-band reduction of a frequency response function. Often, such transient or narrow-band response measures are counterindicative of the broad-band response. Neither of these are appropriate for evaluating LQG compensation, but would be appropriate for L_∞ or H_∞ designs.

Following this argument, the broad-band performance of the LQG_{n_c} and OP designs are plotted against control effort in Figs. 5–9. Each plot is the rms (broad-band) response in a particular performance output y_i as a function of expended rms control effort. The rms control effort is defined as the L_2 norm of the control vector u:

$$\sqrt{\sum_{i=1}^{4} E_\infty(u_i^2)} \tag{57}$$

The performance measures $\sqrt{E_\infty(y_i^2)}$ have been normalized by the open-loop ($u_i = 0$) response. The control effort has been normalized by the effort expended by the OP controller at $\rho = 0.5$. Within each figure, the open symbols correspond to analytical computations, and the solid symbols correspond to experimental measurements.

Each figure also plots for comparison the corresponding full-order LQG performance as a function of control effort. The full-order LQG performance is the analytically best performance achievable for the system at a given level of control effort with a perfect design model of the structure. All OP and LQG_{n_c} designs should be evaluated in comparison to the full-order LQG performance. In particular, the full-order LQG typically resulted in an 80% rms reduction (-14 dB) at actuator saturation for the nominal 1 lb rms disturbance input. This limiting performance reflects the suboptimality of the locations of the sensors and actuators and does not represent any absolute bound for the achievable disturbance rejection for this structure with more sensors and actuators at other locations.

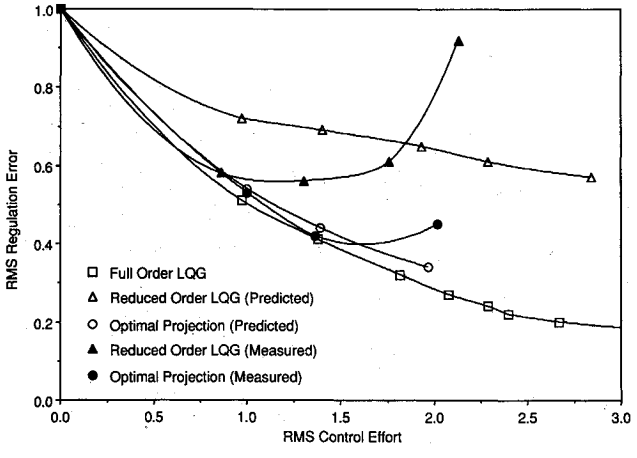

Fig. 5 Experimental and analytical closed-loop rms performance in measure y_1 vs rms control effort.

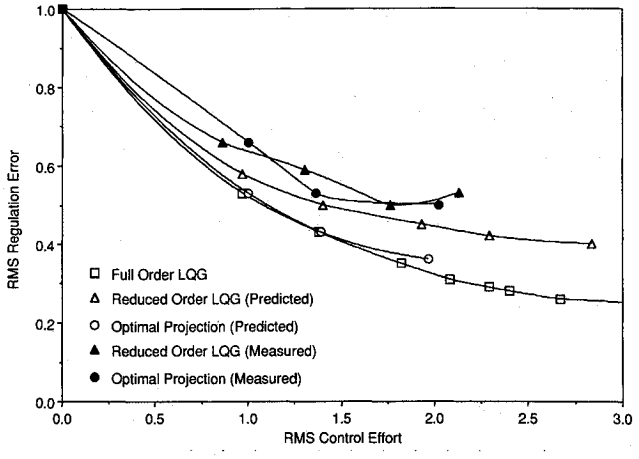

Fig. 7 Experimental and analytical closed-loop rms performance in measure y_3 vs rms control effort.

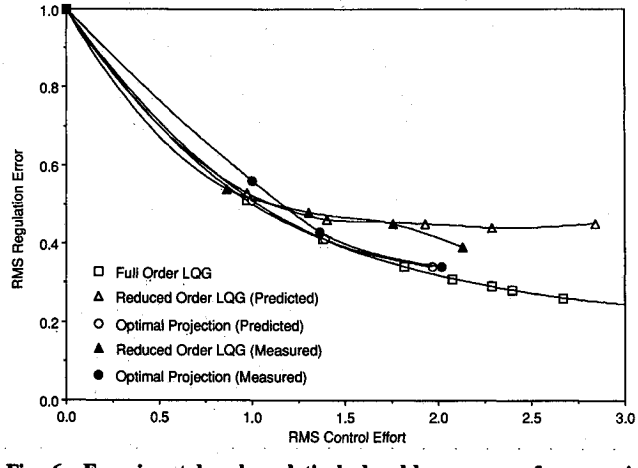

Fig. 6 Experimental and analytical closed-loop rms performance in measure y_2 vs rms control effort.

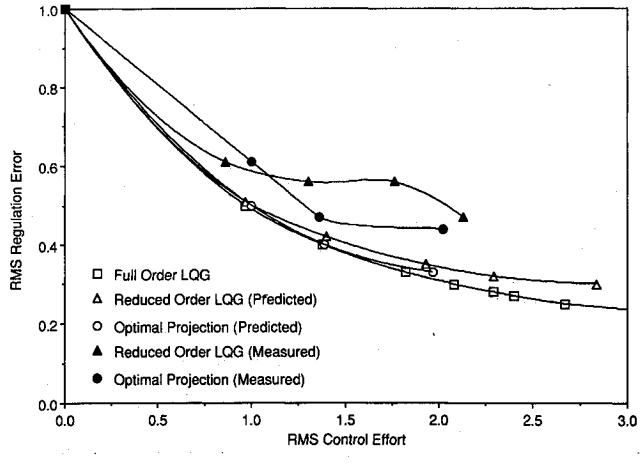

Fig. 8 Experimental and analytical closed-loop rms performance in measure y_4 vs rms control effort.

The performance plots illustrate several important trends.

1) The analytical OP performance is always better than the analytical LQG_{n_c} performance and is very close to the full-order LQG performance. This indicates robustness to model truncation error in the OP designs.

2) The experimental OP performance is usually better than experimental LQG_{n_c} performance. However, both the experimental OP and LQG_{n_c} performance are significantly different from the performance predicted analytically. This indicates a lack of robustness to model parameter errors for both the OP and the LQG_{n_c} designs.

3) The distinction between LQG_{n_c} and OP and between experiment and analysis depends on the performance measure. This means that the sensitivity to model truncation and parameter error is different for each of the performance measures.

The best LQG_{n_c} design is compared to the best OP design in Table 4. For both design methods, the best performance was analytically predicted for $\rho = 0.33$. Overall, the best OP controller is both predicted and observed to perform better than the LQG_{n_c} design. Notice, however, that the performance achieved in the analysis and the experiment differed among the different performance measures. In performance measure y_2, for instance, the OP controller is predicted and observed to have the same response predicted for a perfect, full-order LQG controller. The predicted and observed y_2 responses for LQG_{n_c} design are likewise the same. Thus, performance measure y_2 was robust to any modeling error for both the OP and LQG_{n_c} designs. This could imply that there was little or no significant modeling error in the y_2 direction. On the other hand, the performance measure y_3 for OP is predicted to be 0.36, but it is experimentally measured to be 0.50, the response observed in the LQG_{n_c}. Thus, performance measure was sufficiently sensitive to modeling errors in the OP design that OP and LQG_{n_c} performed equally well in this output.

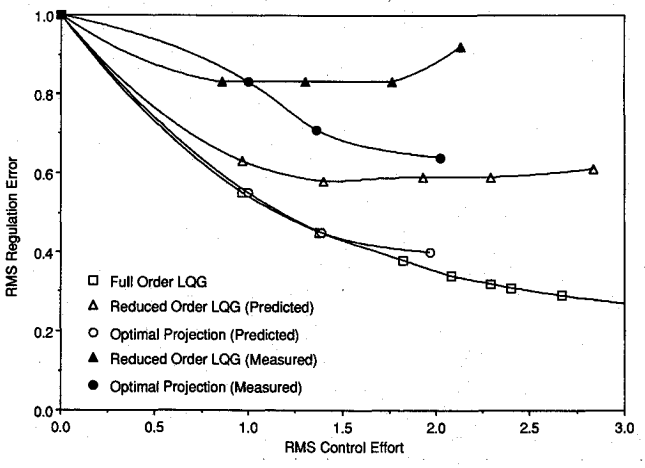

Fig. 9 Experimental and analytical closed-loop rms performance in measure y_5 vs rms control effort.

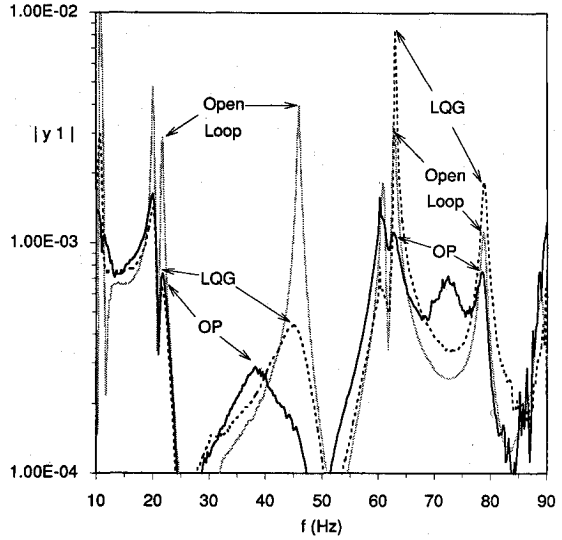

Fig. 10 Experimental frequency response function for y_1 for open-loop, closed-loop LQG_{n_c}, and the closed-loop OP controllers at $\rho = 0.33$.

Table 5 Experimental closed-loop modal damping for $\rho = 0.33$

Mode number	Open loop, %	LQG_{n_c}, %	OP, %
1	0.4	3.5	3.0
2	0.8	—[a]	—[a]
3	0.6	3.0	3.0
4	0.5	4.0	3.0
5	0.5	7.0	10.0
6	0.5	2.5	2.0
7	0.4	0.1	1.0
8	0.6	0.6	1.0

[a]Not identifiable.

Overall, however, LQG_{n_c} did not perform as well as the OP designs. This is apparently due to spillover effects. The best LQG_{n_c} controller was observed experimentally to destabilize modes 7 and above. As shown in Table 5, the LQG_{n_c} controller reduced the modal damping in modes 7 and 8 vis-à-vis the open-loop modal damping, whereas the OP controller consistently added damping to those modes. It is important to realize that mode 7 was *in* the LQG_{n_c} design model. The fact that LQG_{n_c} destabilized this high-frequency mode was undoubtedly due to a lack of parameter robustness even for the modes contained in the design model. This destabilizing nature of the LQG_{n_c} controller was also observed in the frequency response function for the closed-loop response. Figure 10 compares the experimental frequency response function for performance measure y_1 for the LQG_{n_c} and OP controllers against the open-loop response. The LQG_{n_c} closed-loop response peaks corresponding to modes 7 and 8 are all higher than open loop, whereas those for OP are smaller than open loop.

VIII. Conclusions

An optimal reduced-order controller using the optimal projection (OP) formulation has been successfully designed and implemented on an experimental truss structure. By choosing LQG performance weights with the iterative output covariance constraint algorithm, reduced-order optimal controllers were designed that analytically met prespecified rms performance criteria. The achieved broad-band performance from the OP controller was found to be overall better than the comparable suboptimal LQG controller design using a reduced-order model. Experimentally and analytically, the OP controller maintains robustness in performance and stability against truncation modeling errors. However, the experimental data shown here also indicates that the OP controller lacks robustness to model parameter errors. Given the extreme accuracy of the analytical structural dynamic model, this underscores the motivation for robust OP designs even for the relatively modest performance levels attempted here. It also demonstrates the need for *closed-loop appropriate* rather than *open-loop accurate* control design models. Additionally, although the discrete homotopy OP synthesis algorithm was remarkably successful, it may be too slow and inefficient for productive application on larger order systems. It also failed to synthesize high-gain controllers. However, the development of a new continuous homotopy algorithm that is far more efficient promises the routine application of the OP design

method, and its family of fixed-form controller synthesis approaches, to realistic structures. Future research that has been suggested by these results include a systematic examination of the use of robust OP algorithms on realistic structures and the combination of OP with H_∞ constraints. Another area of research concerns how to couple the determination of the design model to the controller synthesis procedure, perhaps using the homotopy parameter β to parameterize the design model as a function of the controller.

Acknowledgments

This work has been supported by Department of Energy Contract DE-AC04-76DP00789 at Sandia National Laboratory. It resulted from a two-year research and development project at Sandia National Laboratories, which involved many individuals. The author specifically recognizes the contributions of J. J. Allen and J. P. Lauffer to the modeling of the structure and implementation of the control designs. Other members of the project team who contributed to the success of the program were A. K. Miller, E. L. Marek, D. W. Lobitz, E. J. Schindwolf, D. O. Smallwood, and V. Gabbard. We also sought and received extremely valuable insight and assistance from R. E. Skelton of Purdue University regarding modeling, weight selection, and synthesis algorithm development. In addition, the homotopy algorithm for the design of the optimal projection controllers could not have been developed without the assistance and guidance of D. S. Bernstein and S. Richter of Harris Corporation.

References

[1]Bernstein, D. S., and Hyland, D. C., "Optimal Projection for Uncertain Systems (OPUS): A Unified Theory of Reduced-Order, Robust Control Design," *Large Space Structures: Dynamics and Control*, edited by S. N. Atluri and A. K. Amos, Springer-Verlag, New York, 1988, pp. 263–302.

[2]Kwakernaak, H., and Sivan, R., *Linear Optimal Control Systems*, Wiley-Interscience, New York, 1972.

[3]Skelton, R. E., *Dynamic Systems Control: Linear Analysis and Synthesis*, Wiley, New York, 1988.

[4]Zames, G., "Feedback and Optimal Sensitivity: Model Reference Transformations, Multiplicative Seminorms, and Approximate Inverses," *IEEE Transactions on Automatic Control*, Vol. AC-26, No. 2, 1981, pp. 301–320.

[5]Francis, B. A., and Doyle, J. C., "Linear Control Theory with an H_∞ Optimality Criterion," *SIAM Journal of Control Optimization*, Vol. 25, No. 4, 1987, pp. 815–844.

[6]Bernstein, D. S., and Haddad, W. M., "LQG Control with an H_∞ Performance Bound: A Riccati Equation Approach," *IEEE Transactions on Automatic Control*, Vol. 34, March 1989, pp. 293–305.

[7]Greeley, S. W., and Hyland, D. C., "Reduced-Order Compensation: Linear-Quadratic Reduction Versus Optimal Projection," *Journal of Guidance, Control, and Dynamics*, Vol. 11, No. 4, 1988, pp. 328–335.

[8]Skelton, R. E., and DeLorenzo, M., "Space Structure Control Design by Variance Assignment," *Journal of Guidance, Control, and Dynamics*, Vol. 8, No. 4, 1985, pp. 454–462.

[9]De Villemagne, C., and Skelton, R. E., "Controller Reduction Using Canonical Interactions," *IEEE Transactions on Automatic Control*, Vol. 33, 1988, pp. 740–750.

[10]Hyland, D. C., and Bernstein, D. S., "The Optimal Projection Equations for Fixed-Order Dynamic Compensation," *IEEE Transactions on Automatic Control*, Vol. AC-29, No. 1984, pp. 1034–1037.

[11]Skelton, R. E., and Hsieh, C., "Covariance Controllers for Dynamic Systems," AIAA Paper 88-4100, Aug. 1988.

[12]Madiwale, A. N., Haddad, W. M., and Bernstein, D. S., "Robust H_∞ Control Design for Systems with Structured Parameter Uncertainty," *Systems and Control Letters*, Vol. 12, 1989, pp. 393–407.

[13]Richter, S. L., and Collins, E. G., Jr., "A Homotopy Algorithm for Reduced-Order Controller Design Using the Optimal Projection Equations," *Proceedings of the Conference on Decision and Control*, Dec. 1989, Tampa, FL, pp. 506–511.

[14]Bailey, T., Gruzen, A., and Madden, P., *RCS/Linear Discrete Actuator Study*, The Charles Stark Draper Lab., Cambridge, MA, AFAL-TR-88-039 and CSDL-R-2075, Aug. 1988.

[15]Peterson, L. D., Allen, J. J., Lauffer, J. P., and Miller, A. K., "An Experimental and Analytical Synthesis of Controlled Structure Design," AIAA Paper 89-1170, April 1989.

[16]Hsieh, C., and Skelton, R. E., "Minimum Energy Controllers Satisfying Inequality Output Variance Constraints," AIAA Paper 88-4167, Aug. 1988.

[17]*PRO-MATLAB User's Guide (v. 3.1)*, The Mathworks, Inc., South Natick, MA, 1987.

[18]Skelton, R. E., "Model Error Concepts in Control Design," *International Journal of Control*, Vol. 49, No. 5, 1989, pp. 1725–1753.

[19]Crawley, E. F., and DeLuis, J., "Use of Piezoelectric Actuators as Elements of Intelligent Structure," *AIAA Journal*, Vol. 25, No. 10, 1987, pp. 1373–1385.

[20]Fanson, J. L., "An Experimental Investigation of Vibration Supression in Large Space Structures Using Positive Position Feedback," Ph.D. Dissertation, California Inst. of Technology, Pasadena, CA, 1987.

[21]*MSC/NASTRAN User's Manual (v. 65)*, MacNeil-Schwindler, Inc., Los Angeles, CA, 1987.

[22]Allen, J. J., and Martinez, D. R., "Automating the Identification of Structural Model Parameters," AIAA Paper 89-1242, April 1989.

[23]Allen, J. J., "NASMAT-A MSC/NASTRAN OUTPUT2 File Interpreter," Sandia National Labs., Albuquerque, NM, 89-0184, 1989.

[24]Richter, S. L., "A Homotopy Algorithm for Solving the Optimal Projection Equations for Fixed-Order Dynamic Compensation: Existence, Convergence and Global Optimality," *Proceedings of the American Control Conference*, June 1987, Minneapolis, MN, pp. 1527–1531.

[25]Richter, S. L., and DeCarlo, R. A., "Continuation Methods: Theory and Application," *IEEE Transactions on Automatic Control*, Vol. AC-28, No. 6, 1983, pp. 660–665.

[26]Hyland, D. C., "The Optimal Projection Approach to Fixed-Order Compensation: Numerical Methods and Illustrative Results," AIAA Paper 83-0303, Jan. 1983.